Geophys. J. Int. (2000) **140,** 101–114

Review of the low-temperature magnetic properties of magnetite from a rock magnetic perspective

A. R. Muxworthy* and E. McClelland

Department of Earth Sciences, University of Oxford, Parks Road, Oxford, OX1 3PR, *UK. E-mail: buffy@earth.ox.ac.uk*

Accepted 1999 August 18. Received 1999 August 12; in original form 1999 March 9

SUMMARY

The low-temperature magnetic properties of magnetite are reviewed, and implications for rock magnetism considered. The behaviour of fundamental properties of magnetite at low temperatures near the Verwey transition (T_v) are documented, and attention is given to various Verwey transition theories. The low-temperature behaviour of the magnetic energies that control domain structure is reviewed in detail. For the first time in rock magnetic literature, the low-temperature anomaly in spontaneous magnetization (M_s) is documented and the differences between the saturation magnetization and M_s near the Verwey transition are discussed. It is argued that the low-temperature behaviour of the magnetocrystalline anisotropy, and in particular the anomaly at T_v, is most likely to affect multidomain remanence during low-temperature cycling. For multidomain crystals it is calculated that the large increase in magnetocrystalline anisotropy intensity and reduction in symmetry on cooling through T_v is likely to reduce the stability of closure domains.

Key words: low-temperature properties, magnetite, rock magnetism.

1 INTRODUCTION

There have been many rock magnetic studies (e.g. Yama-ai *et al.* 1963; Hodych 1990; Özdemir & Dunlop 1998) that have investigated the low-temperature magnetic behaviour of magnetite in the vicinity of the Verwey transition at 120–124 K, T_v (Verwey 1939), and the first cubic magnetocrystalline anisotropy isotropic point at 130 K, T_k (Kakol & Honig 1989). It has been found that, on zero-field cooling of rocks to temperatures below T_v, the magnetic remanence carried by multidomain (MD) magnetite grains partially demagnetizes (e.g. Özdemir & Dunlop 1998). The remaining remanence (memory) is relatively stable (Kobayashi & Fuller 1968; McClelland & Shcherbakov 1995), and the nature and origin of this memory fraction is therefore of great interest to the palaeomagnetist. In order to understand the origin of memory and the processes that govern low-temperature demagnetization (LTD) of MD remanence, it is essential to have a thorough understanding of the low-temperature physics of magnetite, especially of the Verwey transition itself. However, the origin of the Verwey transition is still unclear (Honig 1995; Belov 1996b). In recent years there have been new theories proposed for the Verwey transition which have not been incorporated into rock magnetic models.

* Now at: Institut für Allgemeine und Angewandte Geophysik, München Universität, Theresienstrasse 41 D-80333 München, Germany. E-mail: adrian@rockmag.geophysik.uni-muenchen.de

In this paper, the current theories for the Verwey transition and the low-temperature behaviour of the controlling magnetic energies are reviewed, and the implications for rock magnetism considered. The low-temperature physical properties are examined and discussed, using a combination of theories and experimental results by previous researchers, and complimentary experimental data collected by the authors. Initially, the general physical properties are considered, followed by a review of the low-temperature behaviour of the controlling magnetic energies near T_v, and finally the effects of stress and non-stoichiometry are examined.

2 INTRODUCTION TO THE VERWEY TRANSITION

The first report that magnetite exhibits a low-temperature transition was by Millar (1929), who discovered an anomaly in the heat capacity near 120 K. However, it was Verwey and co-workers (Verwey 1939; Verwey & Haayman 1941; Verwey & Heilmann 1947; Verwey *et al.* 1947) who carried out much of the initial research into the anomalies in both the structure and electrical properties at the transition. Verwey found that there is a slight distortion in the crystal lattice as the structure changes from the inverse-spinel structure above T_v (Okudera *et al.* 1996), to a simpler structure below. Most experimental evidence suggests that the low-temperature structure is monoclinic (e.g. Yoshida & Iida 1979; Zuo *et al.* 1990); however,

there is evidence to indicate that the low-temperature phase lacks a centre of inversion and is triclinic (Miyamoto & Chikazumi 1988; Medrano *et al.* 1999). The unit cell of the commonly proposed monoclinic structure contains four rhombohedrally distorted cubic cells (Fig. 1).

Importantly, at the transition the electrical conductivity drops sharply by a factor of 100, due to a reduction of electron mobility on the B-sublattice (Gleitzer 1997; Fig. 2). Above T_v, electrons from the 3*d* shells move or 'hop' between the Fe^{3+} and Fe^{2+} cations on the B-sublattice, and magnetite behaves like a semiconductor:

$$Fe^{3+} + e^- \Leftrightarrow Fe^{2+}.$$

On cooling below T_v, the hopping is sharply reduced due to a strong increase in the activation energy required for hopping of the electrons. The reduction in electron mobility on the B-sublattice is demonstrated by Mössbauer spectroscopy (Fig. 3; our new data) as follows. The hyperfine fields associated with the two B-sublattices above T_v are indistinguishable to Mössbauer spectroscopy because the frequency of the hopping is considerably greater than the inverse of the Mössbauer measuring time (De Grave *et al.* 1993). As a consequence, the Mössbauer effect sees an average valency state, often denoted as $Fe^{2.5+}$ (e.g. Zhang & Satpathy 1991). Below T_v, the two B-sublattices are distinguishable (Toyoda *et al.* 1999) due to the reduction in the hopping rate (*cf*. the reduction in the conductivity at T_v) (Fig. 2).

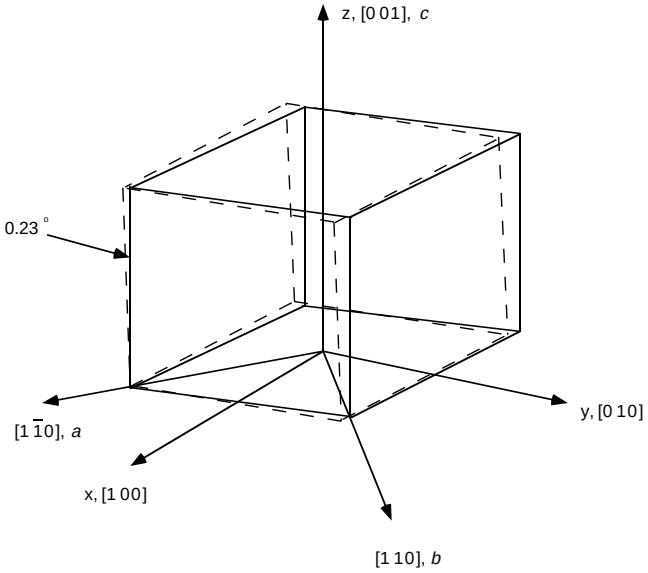

Figure 1. Relationship between the low-temperature monoclinic axes (*a*, *b* and *c*), the rhombohedrally distorted cell (solid line), and the high-temperature cubic unit cell (dashed line). Each monoclinic unit cell consists of four rhombohedrally distorted cells.

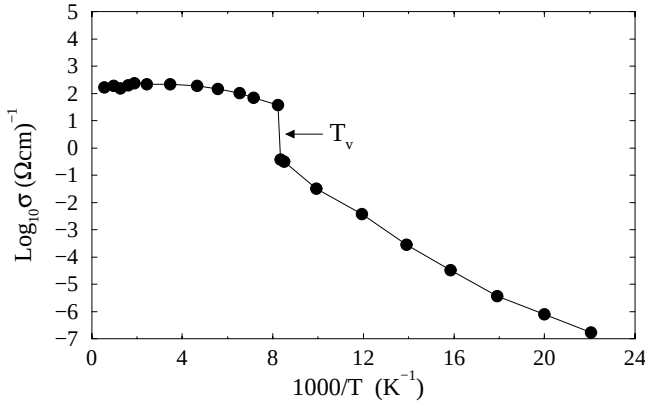

Figure 2. Conductivity of magnetite as a function of temperature. After Gleitzer (1997).

2.1 Brief review of the various Verwey transition theories

Many mechanisms have been proposed to account for the experimental data at T_v; that is, for the structural change, the reduction in the conductivity (Fig. 2) plus anomalies in the heat capacity (Millar 1929; Kozlowski *et al.* 1996), magnetic relaxation processes (Walz & Kronmüller 1991, 1994), the magnetocaloric effect (Belov *et al.* 1982), magnetoresistance (Belov 1994; Gridin *et al.* 1996), spontaneous magnetization M_s (Belov 1993, Fig. 5), magnetocrystalline anisotropy (e.g. Bickford 1949; Bickford *et al.* 1957; Abe *et al.* 1976, Fig. 13), and magnetostriction (e.g. Tsuya *et al.* 1977; Aksenova *et al.* 1987, Fig. 17). It has also been found that variations in stoichiometry (e.g. Aragón *et al.* 1985; Aragón 1992; Honig 1995, Fig. 18) and pressure (Rozenberg *et al.* 1996, Fig. 20) strongly affect the Verwey transition. Unfortunately, there is too much experimental evidence to discuss in detail in this paper. Some of the topics will be discussed in the rest of the text; for the others, the reader is referred to the suggested literature.

Although several theories exist (e.g. Verwey 1939; Cullen & Callen 1971; Honig & Spalek 1992; Belov 1993), none has been able to explain all the experimental data. The various models can be roughly split into two camps: structural-electronic and magneto-electronic. The magneto-electronic model is the more recent of the two models, and is the only theory to incorporate the anomaly in M_s. To the authors' knowledge, the anomaly in M_s has never been previously considered in the rock magnetic literature.

In this paper, the two models are briefly reviewed, and the authenticity of the low-temperature anomaly in M_s, which at present has limited experimental evidence, is validated.

2.2 Structural-electronic model of the Verwey transition

Verwey & Haayman (1941) proposed that the Verwey transition is an ionic order–disorder transition. They suggested that, below T_v, the Coulomb repulsion between neighbouring Fe^{2+} and Fe^{3+} B-sublattice site cations causes the two cations to arrange themselves on alternate (100) planes producing the crystal distortion. According to this model, the reduction in the conductivity is a product of the ionic ordering. Anderson (1956) showed that the Coulomb interaction between the cations on the octahedral sites of ferrites gives rise to short-range order (SRO) and is minimized by $\sim(3/2)^{N_B/2}$ different configurations, where N_B is the number of B sites. A few of these configurations have long-range order (LRO), the Verwey or low-temperature structure being one of these LRO states (Zuo *et al.* 1990). Anderson interpreted the Verwey transition as a loss of LRO upon heating through the transition. Mössbauer and NMR studies (Hargrove & Kündig 1970; Rubinstein & Forester 1971), using more detailed analysis than we present here, identified more Fe^{2+} and Fe^{3+} sites than the

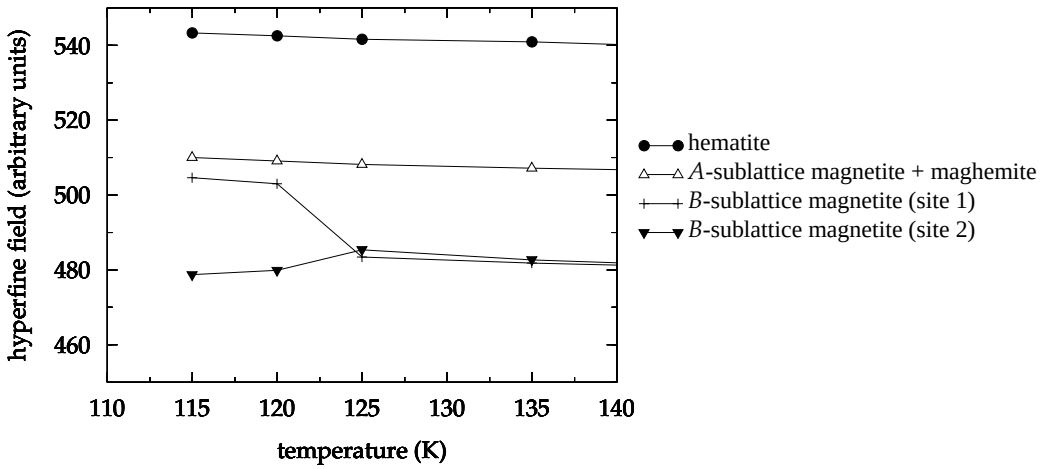

Figure 3. Our measurement of the hyperfine splitting field as a function of temperature for a batch of non-stoichiometric Johnson–Matthey magnetite. The crosses and solid triangles represent the Fe^{2+} and Fe^{3+} ions on the B-sublattice. Above T_v they are indistinguishable; below T_v, they are distinguishable. However, it is unknown which ion causes enhancement or reduction in the hyperfine field (P. Solheid 1997, personal communication). The hyperfine fields associated with the A-sublattice + maghemite and haematite are also shown. They are unaffected by the Verwey transition.

single Fe^{2+} and single Fe^{3+} predicted by the Verwey model. Later, Mizoguchi (1978a) found as many as five different Fe^{3+} sites on the B-sublattice using NMR. As a result, a number of more complicated charge-ordering models have been proposed (e.g. Mizoguchi 1978b; Iida 1980; Zuo *et al.* 1990; Mishra & Satpathy 1993).

2.3 Magneto-electronic model of the Verwey transition

The magneto-electronic model was developed by Belov (1993, 1994, 1996a,b) in response to two important discrepancies between the structural-electronic model and experimental data; namely, the extremely low mobility of the conduction electrons above T_v, which is not explained by the structural-electronic model, and an unexplained anomaly in M_s at the transition.

The number of available hopping electrons is 1.35×10^{22} cm^{-3} (Belov 1993), which is comparable with that which exists in metals, and is much greater than the value in ordinary semiconductors. However, the actual conductivity of magnetite is akin to that of semiconductors (Belov 1993), and so the conduction electrons have very low mobility. Let us consider the origin of this low electron mobility. The Verwey model (Verwey 1939; Verwey & Haayman 1941) assumes a 'hopping' mechanism for electrical conduction in magnetite. An alternative approach has been to apply band theory of electrical conduction to magnetite and other ferrites (e.g. Cullen & Callen 1971, 1973; Samiullah 1995). However, neither of these two models explains the extremely low mobility of the conduction electrons in magnetite above T_v. The low electron mobility has been attributed to the electrostatic interactions discussed previously in the structural-electronic model; however, Belov (1993) notes that this is not sufficient to cause the large reduction in the conductivity. Instead, Belov (1993) points out that in semiconductors there is another important mechanism that causes localization of conduction electrons—the Vonsovskii exchange interaction (Vonsovskii 1946; Nagaev 1971). This is the exchange interaction between valence and inner electrons in ferromagnetic materials. The spin of valence electrons is acted upon by the magnetic field exerted by the internal electrons (Vonsovskii 1946).

The magneto-electronic model applies the Vonsovskii exchange interaction theory to magnetite. The valence electrons are the hopping electrons, and the inner electrons are the fixed electrons on the A- and B-sublattice cations. On cooling through the Verwey transition, the hopping electrons are magnetically ordered under the influence of the Vonsovskii exchange interaction with the magnetic cations, to form an e-sublattice. Because the Vonsovskii exchange interaction between the hopping electrons and the iron cations is negative (antiferromagnetic), this leads not only to localization of the conduction electrons but also to a partial screening of the total magnetic moment (Abrikosov 1968); that is, the e-sublattice electrons align antiparallel to the net magnetic moment of the A- and B-sublattices (Fig. 4), and hence antiparallel to the B-sublattice.

Consequently, there is a small decrease in M_s for $T < T_v$. At $T > T_v$, the thermal motion destroys the magnetization of the e-sublattice, which results in a small experimentally detected anomaly in M_s (Figs 5, 6 and 9). According to theories of Belov (1996a), the interaction of a strong sublattice (A- and B-sublattices) with a weak sublattice (e-sublattice) retards the Verwey transition; that is, the transition is spread over a certain temperature interval (see Figs 5 and 6). This retardation is supported by results from photoemission spectroscopy (Chainani *et al.* 1996). In Belov's sample, the decrease in M_s occurs over a wide temperature range of greater than 100 K. The provenance or purity of this material is not cited by Belov. We find a much sharper anomaly in M_s (see next section) which occurs over less than 15 K, and we suspect that the anomaly may be broadened by impurities in Belov's sample.

The antiferromagnetic Vonsovskii exchange interaction also explains the reduction in electron mobility above T_v. Above

Figure 4. Magneto-electron sublattice electron model. After Belov (1993).

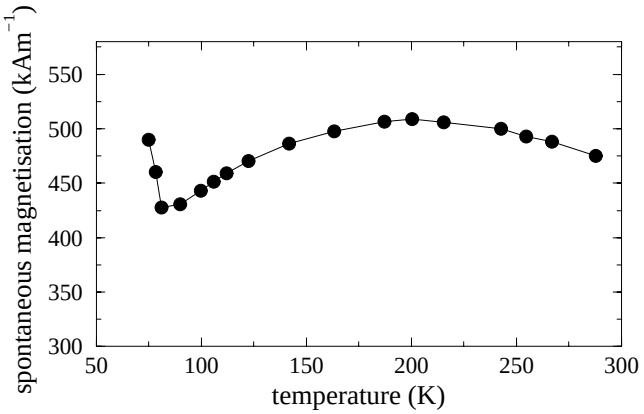

Figure 5. Spontaneous magnetization as a function of temperature for magnetite. Data originally collected by Skipetrova (1978) and reported in Belov (1993).

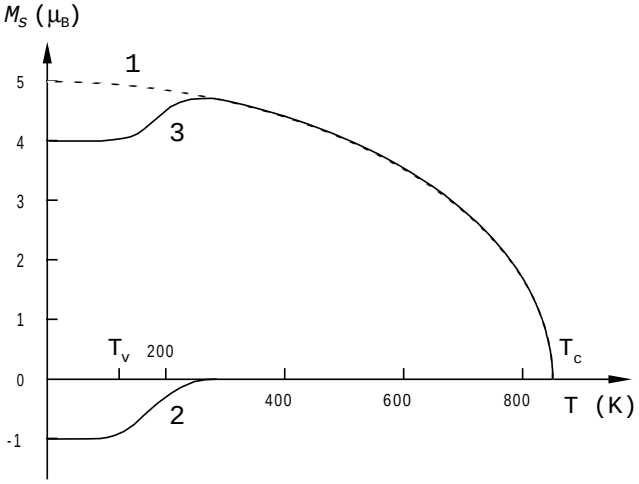

Figure 6. Schematic representation of the spontaneous magnetization of magnetite's temperature dependence at low temperature. Curve 1: total M_s of A- and B-sublattices; curve 2: M_s of e-sublattice; and curve 3: total M_s of A-, B- and e-sublattices. After Belov (1996a).

T_v, the Vonsovskii exchange interaction is insufficient to cause LRO of the hopping electrons; however, it is large enough to affect the orientation of the hopping electrons. Because the Vonsovskii exchange interaction in magnetite is antiferromagnetic, the hopping electrons periodically reverse (flip) their spin during hopping, which requires an additional activation energy (Belov 1996a) and results in a reduction in the electron mobility.

2.4 Differences in spontaneous and saturation magnetization at T_v

The spontaneous magnetization, M_s, is the magnetization within the centre of a domain in zero field. The saturation magnetization, M_{sat}, is the magnetization measured in a saturating field; that is, the field required to make a multi-domain grain single domain (technical saturation). To ensure that technical saturation has been obtained it is common practice to determine M_{sat} by measuring in a field greater than the technical saturation field; for example, magnetite saturates at 0.3 T (Thompson & Oldfield 1986), but M_{sat} is often determined by applying fields greater than this: 0.6 T (Heider *et al.* 1996), 1 T (King 1996) and 1.5 T (Dankers & Sugiura 1981).

In rock magnetic literature, M_s and M_{sat} are often considered to be identical, and are indiscriminately interchanged (e.g. O'Reilly 1984; Dunlop & Özdemir 1997). At room temperature and above, this assumption is valid; however, according to the magneto-electronic model there is a significant difference between the saturation and spontaneous magnetizations at low temperatures below the Verwey transition (Belov 1993). The difference is because of the interaction of the e-sublattice with the external saturating field. The effect of a field on the e-sublattice is two-fold: first if the external field is large enough then the electrons in the e-sublattice align in the direction of the field, and second for even greater external fields the e-sublattice is destroyed; that is, the electrons become delocalized (Belov 1994). Collectively these two processes are termed the 'paraprocess' (Belov 1994). The paraprocess in magnetite reduces the magnetization associated with the e-sublattice, which in effect increases the net magnetization of the entire lattice (see Fig. 4). The paraprocess gives rise to an increase in electron mobility which is documented in magneto-resistance studies (e.g. Belov 1994; Gridin *et al.* 1996). In the low-temperature phase of magnetite, the paraprocess is not significant until fields of the magnitude needed to cause technical saturation are applied (Belov 1993). Therefore, below the Verwey transition M_{sat} measured in a field greater than the minimum field required to cause technical saturation is significantly greater than M_{sat} measured in the minimum field (Belov 1993).

Note that the effect of the paraprocess far outweighs any diamagnetic contribution to M_{sat}. If we take the diamagnetic susceptibility for magnetite to be 1.4×10^{-7} m^3 kg^{-1} (Mulay & Boudreaux 1976) and assume that it is independent of temperature (Dunlop & Özdemir 1997), then, in a field of 1 T, the diamagnetic component contributes a magnetization of approximately 0.1 per cent of the total M_{sat}, whereas the paraprocess contribution is up to 20 per cent.

Because there is very limited experimental data examining the low-temperature behaviour of M_s (Belov 1996b), we have measured the low-temperature variation of M_{sat} in order to test the magneto-electronic theory of Belov (1993). In the remainder of this section, the direct measurement of the saturation magnetization and the determination of the spontaneous magnetization from low-temperature hysteresis loops are reported. There is then a general discussion and comparison of the structural-electronic and magneto-electronic models.

2.4.1 *Measurement of saturation magnetization at T_v*

The saturation magnetization was measured (Fig. 7) by heating a hydrothermal magnetite sample (H (39 μm)) (see Appendix for a description of the samples) from 20 to 300 K in fields above the room temperature technical saturation field ($\approx$0.3 T). This was measured using a Quantum Design Magnetic Property Measurement System (MPMS).

The most immediately obvious feature (Fig. 7) is the sharp jump in M_{sat} at the Verwey transition. This is very much sharper than the anomaly in M_s observed by Belov. Below T_v, increasing the applied field from 0.5 to 0.8 T increases the measured magnetization below T_v, which decreases the size of the sharp anomaly at T_v (Fig. 7). The difference in the size

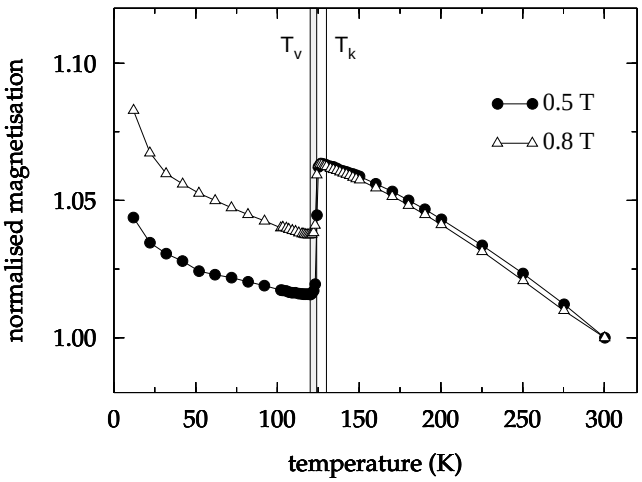

Figure 7. Magnetization of magnetite sample *H* (39 μm) as a function of temperature in the presence of two different applied fields.

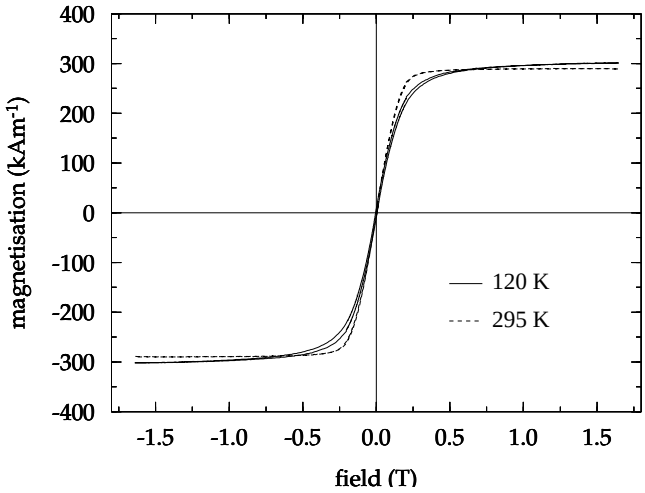

Figure 8. Hysteresis loops for hydrothermal sample *H* (76 μm) at two temperatures.

of the anomaly is due to the paraprocess; that is, below T_v the external field interacts with the e-sublattice, which results in either rotation or delocalization of the e-sublattice electrons. Above T_v the e-sublattice is destroyed by thermal energy. The paraprocess increases with field, and hence M_s increases below T_v, which in turn decreases the size of the sharp jump in the magnetization at T_v. Similar results are reported elsewhere (Domenicali 1950; Matsui *et al.* 1977; Aragón 1992; King 1996). Sampling on single crystals, Domenicali (1950) attributed the anomaly to changes in the magnetocrystalline anisotropy and its control on the preferred direction of magnetization; however, this hypothesis can be rejected because in the present study the sample contained a large number of randomly orientated grains. For randomly orientated grains, the mechanism suggested by Domenicali (1950) would average to zero, and no anomaly would be observed. Matsui *et al.* (1977) and Aragón (1992) both measured at only one applied field (1 T), and both reported an anomaly of $\approx$0.1 per cent in the magnetization at T_v. They postulated that the anomaly is due to small populations of anisotropic ions such as Fe^{1+} and Fe^{2+} in a doublet ground state (Slonczewski 1958; Abe *et al.* 1976); however, this hypothesis does not explain the field dependence of anomaly size, nor has it been experimentally tested.

By incorporating the paraprocess effect, the magneto-electronic theory is the only model at present that can explain the field dependence of the anomaly in M_s at T_v. Our experimental data therefore support this model. In summary, in magnetite the effect of the paraprocess is to increase the net magnetization below T_v. The paraprocess is field-dependent; that is, it increases with increasing field.

2.4.2 *Measurement of spontaneous magnetization at* T_v

The spontaneous magnetization was determined by measuring 29 hysteresis loops at low temperatures between 110 and 300 K using a vibrating sample magnetometer (VSM) at the Institute for Rock Magnetism, Minnesota. Hysteresis loops were measured as a function of temperature for two hydrothermal magnetites, *H* (3.0 μm) and *H* (76 μm) (see Appendix for a description of the samples). Two typical hysteresis loops for the sample *H* (76 μm) are shown in Fig. 8.

At 300 K, technical saturation occurs in fields of $\approx$0.3 T, whereas at 120 K the sample is not magnetically saturated in a field of 1.5 T (Fig. 8). The intensity of magnetization at $\approx$0.5 T for the 120 K hysteresis loop is less than for the same field on the 300 K curve (Fig. 8). The reason for these two differences can be explained by the magneto-electronic model. The difference in intensity for the two loops is due to the presence of the e-sublattice at 120 K, which reduces the net magnetization (Fig. 6). The difference in the saturation field is due to the paraprocess effect: at 300 K the paraprocess effect is very small; however, on cooling to near T_v it becomes significant. The field-dependent paraprocess destroys the e-sublattice, which effectively increases the net magnetization. At 120 K, the paraprocess does not completely saturate until $\approx$1.9 T (Belov 1993, 1996b; unfortunately the maximum reliable field on the VSM used in this study was only 1.6 T), and hence the difference between saturation fields at 120 K and 300 K. Note that, at 120 K, M_s at 1.9 T is slightly greater than at 300 K, due to the reduction in thermal energy, which causes the magnetic moments to precess.

We know that the paraprocess prevents us from directly equating M_s to the measured saturation remanence at temperatures below T_v. The higher the field is above technical saturation, the larger the contribution from the paraprocess; that is, rather than the spontaneous magnetization alone, the spontaneous magnetization plus the effect of the field-dependent paraprocess is measured. In Fig. 9, the magnetization intensity measured on the initial forward curve of a hysteresis loop at four applied fields is plotted against the temperature at which each of the 29 loops was produced. These magnetization values are thus estimates of the spontaneous magnetization, but are enhanced by various amounts due to the paraprocess. The curve for 0.3 T is therefore the closest approximation to the true temperature dependence of M_s. In each curve, the estimated M_s value drops close to the Verwey transition, but this decrease is much larger for the lower-field measurements. If the spontaneous magnetization is calculated from a field substantially greater than the technical saturation field (0.3 T), for example 1.4 T, where the paraprocess is large, then the anomaly in the calculated spontaneous magnetization is significantly reduced.

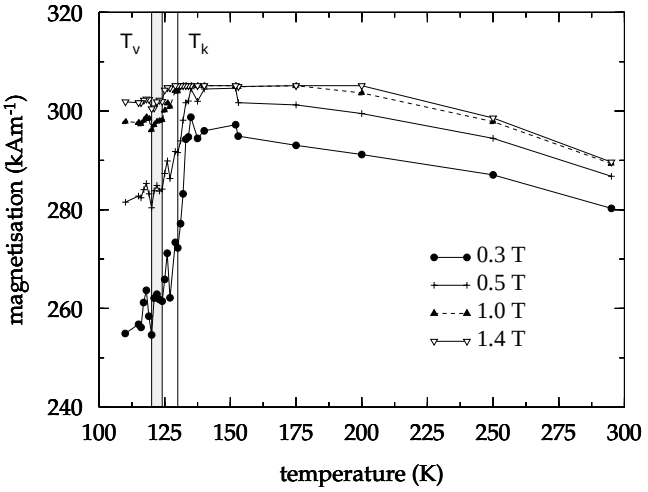

Figure 9. Various calculations of the spontaneous magnetization as a function of temperature for the hydrothermal sample *H* (76 μm). Each curve is calculated from hysteresis loops similar to those shown in Fig. 8. The different curves represent the field value from which M_s is calculated. For example, the '1.0 T' curve is the magnetization at 1.0 T on the initial forward curve in each hysteresis loop. Many hysteresis loops were measured over the temperature range 105 K to room temperature. T_v and T_k are marked, T_v as a range 120–124 K.

The spontaneous magnetization as a function of temperature for the hydrothermal samples *H* (3.0 μm) and *H* (76 μm) is shown in Fig. 10. These two curves were calculated assuming a technical saturation at 0.3 T; in other words, each curve was calculated by taking the value for the magnetization at 0.3 T from hysteresis loops similar to those shown in Fig. 8. At fields less than the technical saturation field, that is $\leq$0.3 T, there is a small contribution from the paraprocess to the magnetization; however, it is difficult to calculate for this. However the effect of the paraprocess contribution in fields less than 0.3 T is to decrease the size of the low-temperature anomaly in the

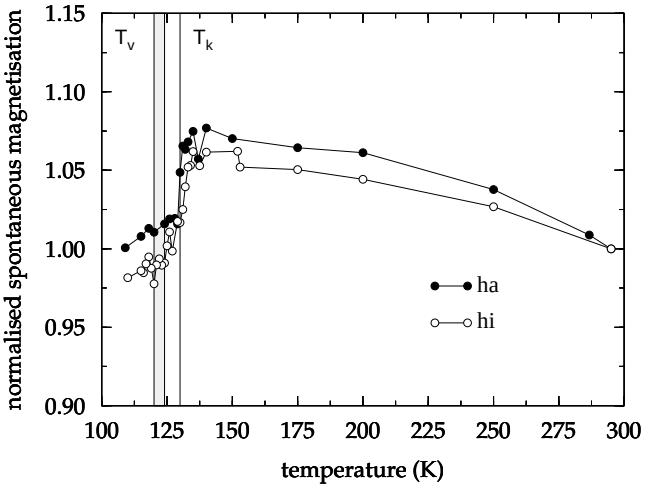

Figure 10. Spontaneous magnetization as a function of temperature for the hydrothermal samples *H* (3.0 μm) and *H* (76 μm). Each curve is calculated by taking the value for the magnetization at 0.3 T from hysteresis loops similar to those shown in Fig. 8. T_v and T_k are marked, T_v as a range 120–124 K.

magnetization at $T < T_v$; in other words, the paraprocess increases the measured magnetization below T_v. Therefore the true spontaneous magnetization for a sample in zero field is larger than that calculated at $H = 0.3$ T.

The spontaneous magnetization measured in this study (Fig. 10) shows a sharper low-temperature anomaly than that measured by Skipetrova (1978; Fig. 5) and reported in Belov (1993). The reason for this difference has not been determined, but may be due to the presence of impurities in Belov's sample. No information is known about the origin of the sample used to determine Fig. 5.

Note that in theory it is possible to simply determine the spontaneous magnetization by measuring the magnetization of a sample in the technical saturation field on heating from below T_v to room temperature. It is, however, more accurate to determine M_s from hysteresis loops measured at a range of temperatures. There are two reasons for this: first, there are uncertainties in a sample's technical saturation field below T_v which can only be determined by measuring its hysteresis loops; and second, by determining M_s from hysteresis loops, any possible contributions to the magnetization caused by heating and cooling a sample in a field below the Verwey transition are removed.

2.5 Comparison of the structural- and magneto-electronic models

Both the structural-electronic and magneto-electronic models have experimental evidence in their favour. Strong support for the structural-electronic hypothesis comes from both Mössbauer spectroscopy (Hargrove & Kündig 1970; Rubinstein & Forester 1971) and NMR (Rubinstein & Forester 1971; Mizoguchi 1978a). For $T > T_v$, Fe^{2+} and Fe^{3+} cations on the B-sublattice are indistinguishable to Mössbauer spectroscopy and NMR; however, on cooling below T_v, they become distinguishable (Fig. 3). This is interpreted by the structural-electronic model as ordering of the Fe^{2+} and Fe^{3+} cations. Belov (1996a), however, provides a second interpretation of Mössbauer spectroscopy and NMR results in terms of the magneto-electronic model. He argues that, at $T < T_v$, the Vonsovskii exchange interaction between the iron cations and the hopping electrons orders the hopping electrons to form the e-sublattice. This localization gives rise to different values of H_{hf} for Fe^{2+} and Fe^{3+} cations of the B-sublattice (Fig. 3). At $T > T_v$, where the magnetic order is partially destroyed, hopping electrons delocalize and migrate between the Fe^{2+} and Fe^{3+} cations, creating an averaged H_{hf} field (Fig. 3).

In favour of the magneto-electronic model, there are anomalies at T_v in the spontaneous magnetization (Figs 5, 9 and 10), the magnetocaloric effect (Belov 1982) and the magnetoresistance (e.g. Belov 1994; Gridin *et al.* 1996), which have only been explained by the magneto-electronic model. Belov (1993) attributes the distortion in the cubic symmetry below T_v, which is fundamental to the structural-electronic model, to the changes in the anisotropic magnetostriction. The magneto-electron model can also explain the dependence on field during low-temperature cooling—samples cooled in large fields show a different behaviour at T_v compared to samples cooled in a zero field (Domenicali 1950; Moskowitz *et al.* 1993). Most other effects, for example anomalies in the magnetocrystalline anisotropy (e.g. Abe *et al.* 1976), have been explained by both theories.

In summary, there is strong experimental support for both the magneto-electronic model and the structural electronic model; however, the anomaly in M_s at T_v is only accounted for by the magneto-electronic model. Because the behaviour of M_s is fundamental to the magnetic domain structure, the magneto-electronic approach is preferred in the explanation of other magnetic phenomena of interest to this paper. In low-field and remanence studies, which are of interest to the rock magnetist, it is important to know the behaviour of the spontaneous magnetization rather than that of the saturation magnetization.

3 BEHAVIOUR OF MAGNETIC ENERGIES AT LOW TEMPERATURES

To understand the demagnetization processes that occur at the Verwey transition, it is important to know how the controlling magnetic energies behave near the Verwey transition, namely exchange, self-demagnetizing and anisotropy, and other parameters. The magnetic behaviour of a material is governed by the ascendancy of the controlling magnetic energies—the exchange energy, E_{ex}, the demagnetizing energy, E_d, the anisotropy energy, E_{anis}, and the external field energy, E_h. The total magnetic energy, E_{tot}, is given by

$$E_{tot} = E_{ex} + E_d + E_{anis} + E_h . \quad (1)$$

In this section, the low-temperature behaviours of the controlling magnetic energies are briefly reviewed, and the relative importance of each of the various magnetic energies considered.

3.1 Exchange energy

Experimental evidence (e.g. Alperin *et al.* 1967; Torrie 1967) suggests that the exchange energy is not affected by the Verwey transition, and does not vary significantly from the room temperature value. It should be noted that the exchange integral, which controls the exchange energy E_{ex}, is not the same as the Vonsovskii exchange integral, which gives rise to the anomaly in M_s at T_v (Fig. 5). The two exchange interactions are mutually independent. It is therefore possible for M_s to display a low-temperature anomaly, and for the exchange energy not to do so.

3.2 Self-demagnetizing energy

The magnetostatic energy E_d is given by

$$E_d = -\frac{\mu_0 M_s}{2} \sum_{i=1}^{n} \mathbf{H}_{d,i} \cdot m_i \Delta^3 , \quad (2)$$

where $\mathbf{H}_{d,i}$ is the magnetic field at the location m_i due to each magnetic dipole in the system. The demagnetizing energy depends on M_s, which displays an anomaly at T_v (Fig. 5).

3.3 Anisotropy energy

The total anisotropy energy E_{anis} is the sum of the magnetocrystalline anisotropy energy E_k, the magnetostrictive anisotropy energy E_{strict}, and the magnetoelastic anisotropy E_{me} (Lee 1955):

$$E_{anis} = E_k + E_{strict} + E_{me} . \quad (3)$$

3.4 Magnetocrystalline anisotropy energy

3.4.1 $T_v < T < 300$ K

The cubic magnetocrystalline anisotropy E_k^c is given by (Kittel 1949)

$$E_k^c = K_1(\alpha_1^2\alpha_2^2 + \alpha_2^2\alpha_3^2 + \alpha_3^2\alpha_1^2) + K_2\alpha_1^2\alpha_2^2\alpha_3^2 + \ldots , \quad (4)$$

where K_1 and K_2 are the first two cubic anisotropy constants, respectively, and α_i is the directional cosine of the magnetization vector with respect to the cubic axes. For cubic magnetocrystalline anisotropy there are three easy axes. The behaviour of the magnetocrystalline anisotropy energy at low temperatures is still under debate. Are the isotropic point in the first magnetocrystalline anisotropy constant K_1 at 130 K (Bickford *et al.* 1957; Fig. 11) and the Verwey transition at $\approx$120–124 K two separate low-temperature transitions or just

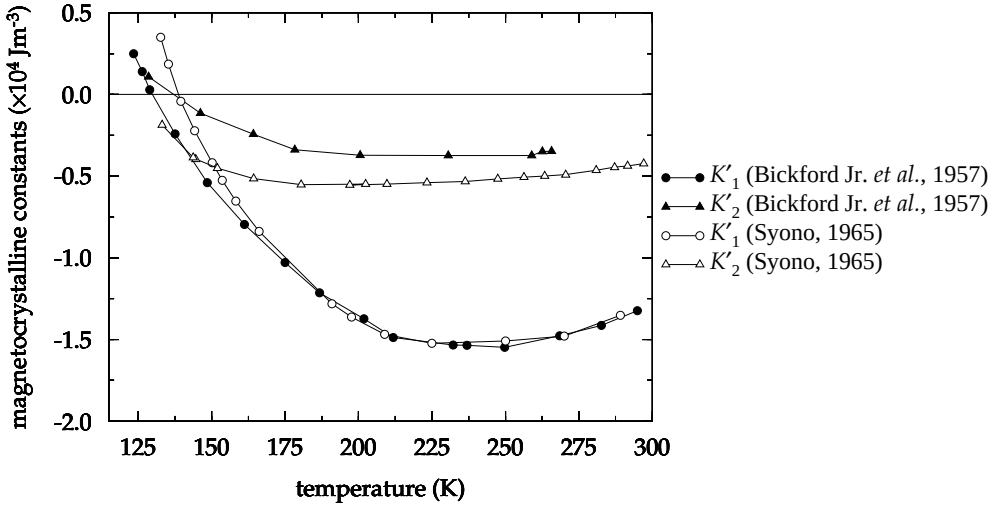

Figure 11. Magnetocrystalline anisotropy constants K_1' and K_2' as a function of temperature showing the large difference in the values of Bickford *et al.* (1957) and Syono (1965).

one? King (1996) argues that they are actually identical, and any discrepancies between the two temperatures is due to the neglect of the second anisotropy constant K_2 and other higher-order contributions. K_2 is usually ignored because K_1 dominates at and above room temperature; however, at the K_1 isotropic point the contribution from K_2 becomes significant.

The two most complete sets of low-temperature magnetocrystalline anisotropy data (i.e. Bickford *et al.* 1957; Syono 1965; Fig. 11) are for K_1' and K_2'; that is, K_i plus a magnetostrictive contribution (Ye *et al.* 1994). In theory, it is possible to obtain K_i by either direct measurement using ferromagnetic resonance (FMR) as suggested by Ye *et al.* (1994), or by simply removing the experimentally measured magnetostrictive term from K_i' (e.g. Kakol *et al.* 1991; Sahu & Moskowitz 1995). With regard to FMR, however, the data sets are rather sparse (Bickford 1949, 1950) in the temperature range $T_v < T \leq$ room temperature. The second method of calculating K_i' is fraught with errors, because for magnetite the values of the magnetostrictive constants are often smaller than the error in the measurement of K_i'.

Using the data of Syono (1965; Fig. 11), King (1996) shows that, by adding K_1' and K_2', the isotropic point is decreased from 139 K for K_1' to 134 K for $K_1' + K_2'$. However, if a similar approach is taken with the data collected by Bickford *et al.* (1957; Fig. 11), then the value for the isotropic point is greater for $K_1' + K_2'$ than for K_1' alone. This raises the possibility that the magnetocrystalline anisotropy E_k is zero at a temperature higher than 130 K, rather than lower, as King (1996) suggests. The reason for the high isotropic point for K_1' measured by Syono (1965; Fig. 11) is unclear. King (1996) suggested that it was due to impurities; however, it is shown below that the effect of small deviations from stoichiometric magnetite is to decrease the isotropic point. It is not until $x \approx 0.4$ for $Fe_{3-x}Ti_xO_4$, that the isotropic point increases to above 130 K (Syono 1965; Kakol *et al.* 1991).

By examining the relative magnetic initial permeability ($\equiv \chi + 1$), Aragón *et al.* (1985; Fig. 12) have produced very strong evidence in support of the two-transition hypothesis. Aragón *et al.* (1985) associate the vertical anomaly with the Verwey transition, and the change in slope from $y = x$ to the horizontal at ≈ 130 K with the isotropic point. It appears in

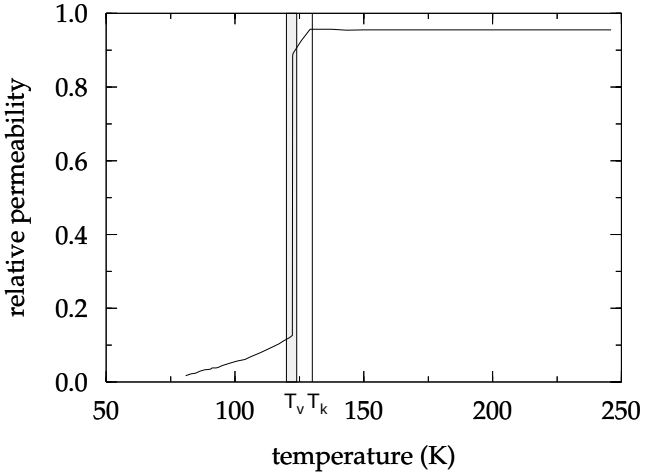

Figure 12. Relative magnetic initial permeability ($\equiv \chi + 1$) as a function of temperature for annealed magnetite single crystal. After Aragón *et al.* (1985). The two transitions T_v and T_k are marked.

answer to the initial question, that the magnetocrystalline isotropic point and the Verwey transition are separate transitions, and not the same as suggested by King (1996).

3.4.2 $T \leq T_v$

Below T_v, the crystal structure transforms from cubic to a less symmetric structure, usually thought to be monoclinic with a tilt from the c-axis of 0.23° (Fig. 1). For the monoclinic low-temperature structure, the magnetocrystalline energy E_k^m is expressed by (Abe *et al.* 1976)

$$E_k^m = \kappa_a + \alpha_a^2\kappa_b\alpha_b^2 + \kappa_{aa}\alpha_a^4 + \kappa_{bb}\alpha_b^4 + \kappa_{ab}\alpha_a^2\alpha_b^2 - \kappa_u\alpha_{111}^2, \quad (5)$$

where α_a, α_b and α_{111} are the direction cosines of the magnetization with respect to the monoclinic a-, b- and cubic [111] axes respectively (see Fig. 1 for co-ordinate system). Abe *et al.* (1976) added the $\kappa_u\alpha_{111}^2$ term to the expression originally derived for an orthorhombic phase by Calhoun (1954), to deal with the small rhombohedral distortion.

The temperature-dependent behaviour of magnetocrystalline constants for both the cubic and monoclinic phases is shown in Fig. 13. Again the magnetocrystalline anisotropy 'constants' in Fig. 13 are not κ_i but κ_i', i.e. κ_i plus a magnetostrictive contribution. The low-temperature monoclinic magnetocrystalline anisotropy constants are considerably larger than the cubic magnetocrystalline anisotropy constants (Fig. 13). The controlling monoclinic constant κ_a' is approximately 10 times greater than K_1'. Consequently, the relative importance of the monoclinic magnetocrystalline anisotropy to the domain structure is far greater than the cubic magnetocrystalline anisotropy; that is, $E_k^m \gg E_k^c$. This abrupt jump in the magnetocrystalline anisotropy on cooling through T_v is expected, because the magnetocrystalline anisotropy is controlled by the mobility of the Fe^{2+} ions (or alternatively the mobility of the hopping electrons) (Fletcher & O'Reilly 1974; Belov 1993). As the mobility decreases, the magnetocrystalline anisotropy increases (Belov 1993).

There is also a significant reduction in the symmetry of the magnetocrystalline anisotropy field. We have depicted the magnetocrystalline energy fields for $T = 290$, 126 and 110 K in Figs 14, 15 and 16. In the cubic phase, for $T > 130$ K the easy-axis is the [111] (Fig. 14), and for $T_v < T < 130$ K, K_1' is positive, which switches the easy-axis from the [111]-axis to the [100] (Fig. 15). The monoclinic magnetocrystalline anisotropy has a lower order of symmetry than the cubic phase, the easy-axis is the c-axis; however, the b-axis is also relatively easy compared to the a-axis (Fig. 16).

3.5 Magnetostrictive and magnetoelastic anisotropy energies

The cubic magnetostrictive energy, E_{strict}^c represents the interaction between the magnetic anisotropy and strain, and is given by (Kittel 1949)

$$\begin{aligned} E_{sriict}^c &= [(9/4)(c_{11} - c_{12})\lambda_{100}^2 - (9/2)c_{44}\lambda_{111}^2] \\ &\quad \times (\alpha_1^2\alpha_2^2 + \alpha_2^2\alpha_3^2 + \alpha_3^2\alpha_1^2) \\ &= K_{stict}(\alpha_1^2\alpha_2^2 + \alpha_2^2\alpha_3^2 + \alpha_3^2\alpha_1^2), \end{aligned} \quad (6)$$

where

$$\lambda_{100} = -\frac{2}{3}\frac{B_1}{c_{11} - c_{12}}, \qquad \lambda_{111} = -\frac{1}{3}\frac{B_2}{c_{44}},$$

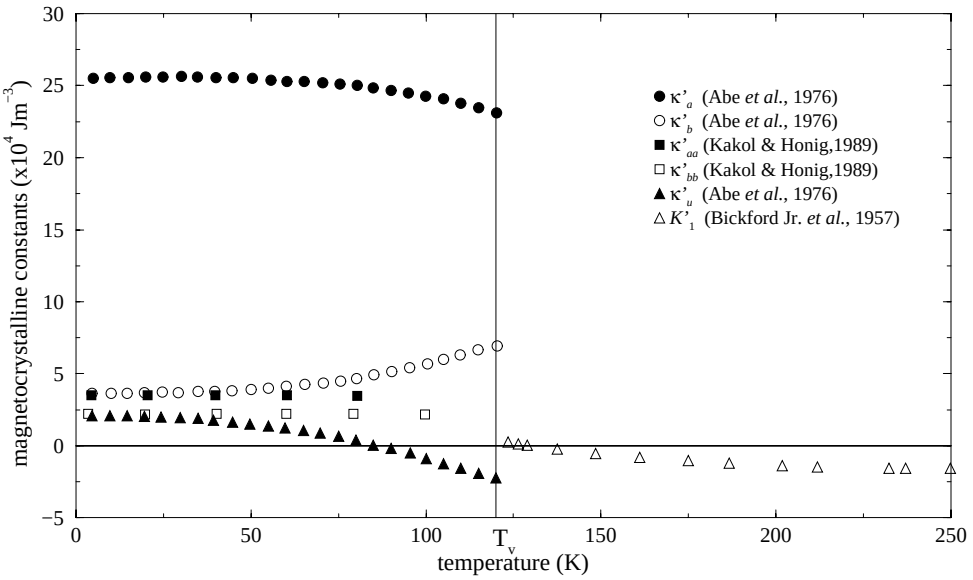

Figure 13. Temperature dependence of the cubic and monoclinic magnetocrystalline constants used in the model. K_1' is the first cubic magnetocrystalline anisotropy constant (eq. 4), and κ_i' are the low-temperature monoclinic constants (eq. 5).

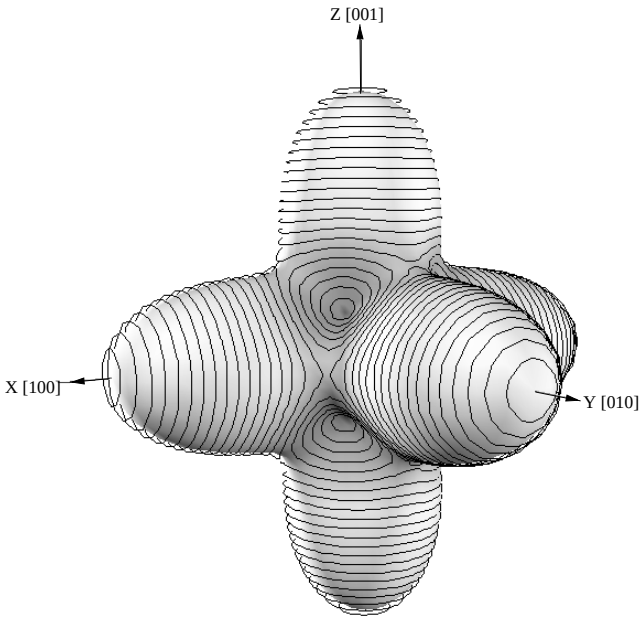

Figure 14. The cubic magnetocrystalline anisotropy of magnetite at 290 K. The hard axes are in the [100], [010] and [001] directions.

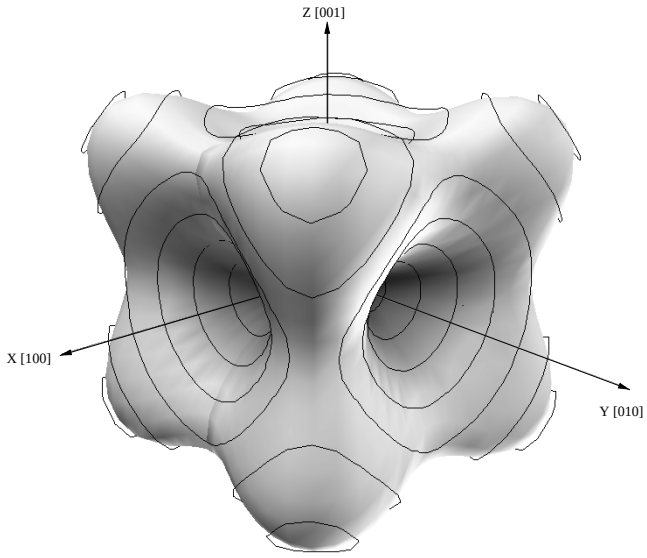

Figure 15. The cubic magnetocrystalline anisotropy of magnetite at 126 K. The hard axis is in the [111] direction.

where c_{11}, c_{12} and c_{44} are elastic moduli, λ_{100} and λ_{111} are the cubic magnetostriction anisotropy constants for the [100] and [111] crystallographic directions, respectively, and B_1 and B_2 are the magnetoelastic coupling constants defined by Kittel (1949). The cubic magnetoelastic energy or cubic magnetoelastic coupling energy, E_{me}^c, is given by (Träuble 1969)

$$E_{me}^c = -(3/2)\lambda_{100}(\alpha_1^2\sigma_{11} + \alpha_2^2\sigma_{22} + \alpha_3^2\sigma_{33}) - 3\lambda_{111}(\alpha_1\alpha_2\sigma_{12} + \alpha_2\alpha_3\sigma_{23} + \alpha_3\alpha_1\sigma_{31}), \quad (7)$$

where σ_{ij} is the stress tensor.

It can be seen from eqs (6) and (7) that the magnetostrictive and magnetoelastic anisotropy energies are both controlled by the behaviour of the magnetostrictive anisotropy constants.

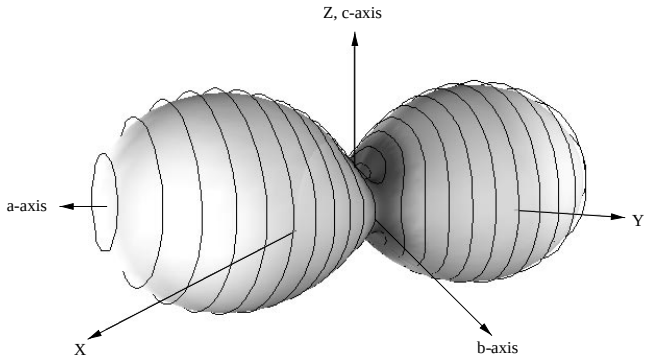

Figure 16. The monoclinic magnetocrystalline anisotropy of magnetite at 110 K. The hard axis is the *a*-axis.

The magnetostrictive energy is also dependent on the behaviour of the elastic moduli c_{11}, c_{12} and c_{44} (eq. 6). It should be noted that the cubic magnetostrictive constants λ_{100} and λ_{111} are defined in terms of c_{11}, c_{12} and c_{44} (eq. 6).

3.5.1 *Behaviour of the elastic moduli at T_v*

Softening anomalies at T_v have been found for c_{11} and c_{44} (Siratori & Kino 1980; Isida *et al.* 1996). The anomaly in c_{44} is much larger than the reported anomaly found in c_{11} (Isida *et al.* 1996). c_{12} is relatively unaffected by the Verwey transition (Siratori & Kino 1980).

A decrease in the elastic moduli reduces the magnetostrictive energy term (eq. 6); however, it also increases the magnetostrictive constants.

3.5.2 *Magnetostrictive anisotropy constants at T_v*

The temperature-dependent behaviour of the magnetostrictive constants of magnetite between room temperature and T_v has been well documented (e.g. Domenicali 1950; Belov *et al.* 1985); however, there have been fewer studies examining the low-temperature behaviour as a function of temperature (Arai *et al.* 1976; Tsuya *et al.* 1977).

The monoclinic magnetostrictive anisotropy is defined in terms of nine mutually independent constants below T_v (Arai *et al.* 1976); however, it is possible crudely to define the low-temperature magnetostrictive constants in terms of the high-temperature constants λ_{100} and λ_{111} (Arai *et al.* 1976; Tsuya *et al.* 1977). This gives some estimate for the behaviour of the magnetostrictive constants across T_v.

The temperature dependence of all the constants becomes steeper, almost asymptotic, towards the transition (Fig. 17). The anomalies in λ_{100} and λ_{111} across T_v (Fig. 17) have been attributed to reduction of the elastic moduli (Aksenova *et al.* 1987); however, there must also be temperature variations in the magnetoelastic coupling constants (B_1 and B_2, eq. 6) to explain the behaviour of the λ_{100} and λ_{111}.

In summary, the magnetostrictive and magnetoelastic anisotropy energies are both effected by the Verwey transition; however, on comparison with the magnetocrystalline anisotropy (Fig. 13), the change in intensities of λ_{100} and λ_{111} (Fig. 17) are considerably smaller than the changes in the magnetocrystalline anisotropy constants.

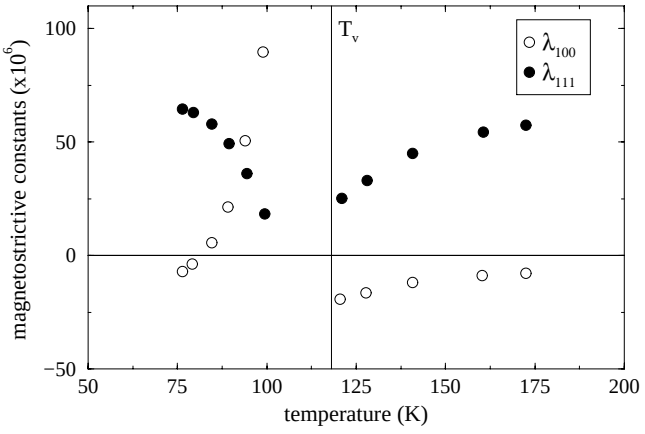

Figure 17. Temperature dependence of the magnetostriction constants across T_v. Above T_v, λ_{100} and λ_{111} are directly measured. Below, they are calculated from the seven low-temperature constants, which gives a rough estimate for the temperature dependence of the magnetostrictive constants. After Tsuya *et al.* (1977).

4 VARIABLE STOICHIOMETRY AT LOW TEMPERATURES

Before 1984, the importance of stoichiometry had not been realized (Honig 1995). In the past 10 years, there have been many investigations that have examined the effect of non-stoichiometry at low temperatures (e.g. Aragón *et al.* 1985; Kakol *et al.* 1991; Aragón 1992; De Grave *et al.* 1993; Kozlowski *et al.* 1996).

4.1 Effect of variable stoichiometry on the Verwey transition

Deviations from stoichiometric magnetite, either by an oxygen deficiency ($Fe_{3(1-\delta)}O_4$) or an impurity, for example $Fe_{3-x}Ti_xO_4$, shift the Verwey transition to lower temperatures (Fig. 18). Non-stoichiometry also depresses and broadens the transition (Honig 1995; Dunlop & Özdemir 1997).

There is a discontinuous anomaly in the Verwey temperature at $\delta = 0.0039$, i.e. $3\delta = 0.012$, which has led to a reclassification (Aragón 1992) of the Verwey transition into first order ($-0.0005 \leq \delta < \delta_c \equiv 0.0039$) and second order ($\delta_c < \delta < 3\delta_c$). For $\delta \approx 3\delta_c$, the magnetite-maghemite/haematite phase boundary is reached and the Verwey transition disappears (Honig 1995). There is a corresponding system for impurities with $x = 3\delta$, for example $Fe_{3-x}Ti_xO_4$, and similarly for $x \geq 9\delta_c$ no Verwey transition has been found (Honig & Spalek 1992; Kozlowski *et al.* 1996).

There have been several structural-electronic theories to explain the effect of the non-stoichiometry on the Verwey transition. The microscopic order–disorder model developed by Honig and co-workers (e.g. Honig & Spalek 1992; Honig 1995) proposes that at the first- and second-order transition, i.e. $\delta = \delta_c$, the Fe^{2+} and Fe^{3+} B-sublattice cations are rearranged to minimize the free energy (Aragón 1992; Honig 1995). This theory has been very successful in explaining the experimental data.

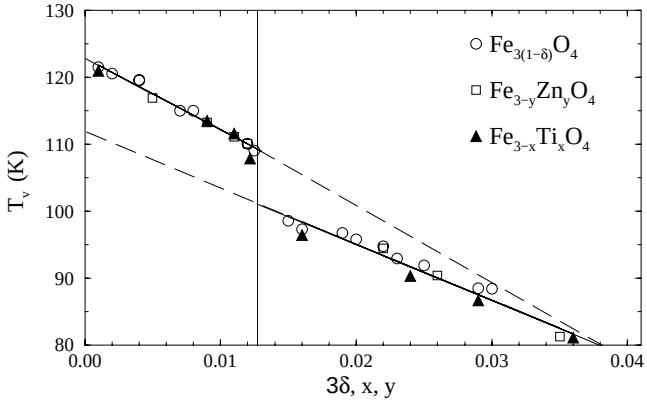

Figure 18. Variation of the Verwey transition temperature T_v with compositions of $Fe_{3(1-\delta)}O_4$, $Fe_{3-y}Zn_yO_4$ and $Fe_{3-x}Ti_xO_4$. After Honig (1995).

The magneto-electronic model has not been explicitly applied to this problem, but it seems reasonable to assume that, as x or δ increases, the negative Vonsovskii exchange interaction between the e-sublattice and A- and B-sublattices weakens. Because the temperature of the Verwey transition is governed by the balance between the Vonsovskii exchange interaction and thermal energy, a decrease in the Vonsovskii exchange interaction causes T_v to decrease. However, this does not explain the first- and second-order effects.

4.2 Effect of variable stoichiometry on the magnetic anisotropy below room temperature

For titanomagnetites ($Fe_{3-x}Ti_xO_4$), the anisotropy constant K_1' passes through a minimum at $x = 0.2$, irrespective of temperature (Syono 1965; Kakol *et al.* 1991; Fig. 19). This coincides with the point where Fe^{2+} ions appear in the tetrahedral interstitial sites. For $x \geq 0.2$, there is a large magnetostrictive contribution to the anisotropy which dominates at high x (Kakol *et al.* 1991). The isotropic point for K_1' decreases from 130 K for magnetite (Kakol *et al.* 1991) until $x = 0.2$, where K_1' is still negative at 77 K (Fig. 19). Note that for $x \geq 0.04$ there is no Verwey transition (Fig. 18). For $x > 0.2$, both the magnetocrystalline anisotropy and the temperature of the isotropic point increase with x (Fig. 19). For high values of x, i.e. $x \approx 0.6$, K_1 is positive between 77 K and T_c (Kakol 1990; Sahu & Moskowitz 1995). Similar results have been found for $Fe_{3-x}Co_xO_4$ (Slonczewski 1958).

5 IMPORTANCE OF STRESS ON THE VERWEY TRANSITION

Around internal dislocations, there are residual stress fields which interact with the magnetization (Träuble 1969). It is therefore important to understand the effect of stress on the behaviour of the Verwey transition. By directly applying external stress it is possible to calculate the behaviour of the controlling magnetic energies at low temperatures.

5.1 External stress at the Verwey transition

By examining the conductivity, Rozenberg *et al.* (1996) have shown that applying external stress to magnetite affects the temperature behaviour of the Verwey transition in a similar manner to variations in the stoichiometry; that is, the Verwey transition decreases with increased stress and is split into first- and second-order phases (Fig. 20). In the pressure range 0–6 GPa, T_v decreases continuously with pressure P from 122 to 107.5 K (Fig. 20). At $P \approx 6$ GPa there is a discontinuous jump in T_v from 107.5 to 100 K; thereafter, for $6 \leq P \leq 12.5$ GPa, there is second-order phase which decreases linearly to 83 K for 12.5 GPa. For $P > 12.5$ GPa no Verwey transition is observed; that is, there is no discontinuous drop in conductivity at low temperatures.

The structure of the low-temperature phase at $P > 12$ GPa is unknown; it is possible that the high pressure actually suppresses the phase transition. Rozenberg *et al.* (1996) explain their results in terms of a simple 'Wigner structure'-type model rather than the order–disorder formulation.

The behaviour of the elastic modulus c_{11} at T_v is strongly affected by external pressure, vanishing completely at T_v for pressures of ≈ 1.2 GPa (Isida *et al.* 1996). c_{12} and c_{44} are unaffected by pressure changes.

5.2 Internal residual stress at the Verwey transition

Assuming the results from external pressure studies are applicable to internal stress, that is stress fields around dislocations, the results of Rozenberg *et al.* (1996) have implications for magnetic domain structures: first, stressed areas of a grain near dislocations will have lower Verwey transition temperatures than stress-free areas; and second, differences in the elastic moduli responses to pressure will increase the anisotropic energy.

The effect of internal stress on the Verwey transition has been studied by King (1996) and Sahu (1997). King (1996) induced internal stress to his lithographic samples by quenching them from 600 °C at rates ≥ 30 °C s^{-1} and by piston pressing. By examining the demagnetization of low-temperature induced SIRM at T_v, he found that the stressed samples displayed a broader, less well-defined Verwey transition than the unstressed samples. This difference in low-temperature behaviour can be explained by a wider range of Verwey temperatures within the sample due to inhomogeneous internal stress.

6 CONCLUSIONS AND IMPLICATIONS FOR ROCK MAGNETISM

At ≈ 120–124 K, magnetite passes through a transition called the Verwey transition, which is due to the reduction in hopping

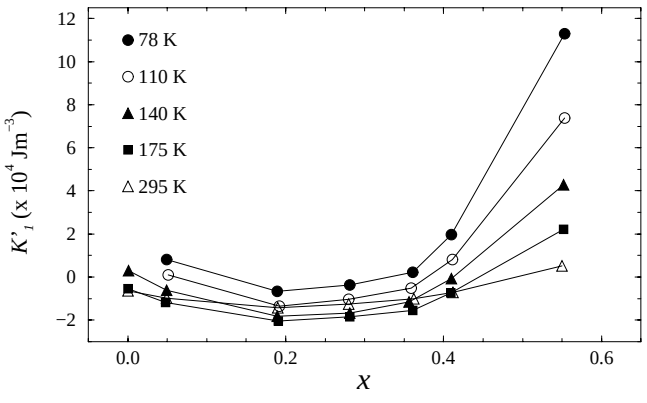

Figure 19. Anisotropy parameter K_1' against x parameter in $Fe_{3-x}Ti_xO_4$ at selected temperatures in the 77–295 K range. After Kakol *et al.* (1991).

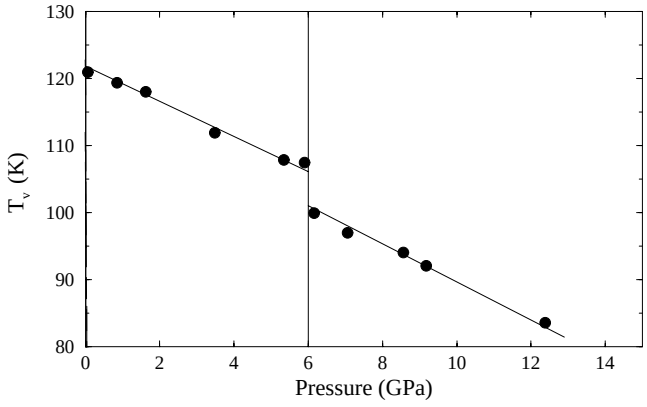

Figure 20. Pressure variation of the Verwey transition. After Rozenberg *et al.* (1996).

electrons. At ≈ 130 K, the first cubic magnetocrystalline anisotropy tends to zero. We argue that the T_k and T_v transitions are separate phenomena, in disagreement with King (1996).

Associated with the reduction in electron mobility at T_v are anomalies in all the controlling magnetic energies except the exchange energy. Of the anomalies in the controlling magnetic energies, the most significant is the large increase in intensity of the magnetocrystalline anisotropy and the reduction in its symmetry, which will strongly affect MD domain structures and their stability. It is possible to estimate the effect on the domain structure by considering the likelihood of closure domains.

An approximate estimate of the favourability of closure domains is found by considering the relative anisotropy, Q (Rave *et al.* 1998). If $Q \geq 1$, then closure domains are unfavourable. Muxworthy & Williams (2000) calculated Q as a function of temperature for magnetite: at room temperature $Q \approx 0.09$, but at 100 K $Q \approx 1$. Therefore at room temperature closure domains are highly favourable for large grains of magnetite with many domains; however, in the monoclinic phase closure domains become less favourable. The stability of the domain structure increases, and this is reflected in the decrease in χ and the increase in H_c on cooling through T_v (Schmidbauer & Keller 1996; Moskowitz *et al.* 1998). This is in agreement with the only published low-temperature domain observation study (Moloni *et al.* 1996), which found that classic closure domains observed at room temperature, for example closure domains with wall angles of 180°, 109° and 71°, re-ordered on cooling through the Verwey transition. At 77 K only planar 180° domain walls aligned in the *c*-plane were observed, or wavy domain patterns usually associated with an out-of-plane easy-axis, but no closure domain structures. The closure domains were seen to return on warming to room temperature, although different surface domain patterns were observed. The question whether it is the anomalous behaviour of the magnetocrystalline anisotropy at T_v or the magnetocrystalline anisotropy at T_k that controls LTD is considered in the companion paper Muxworthy & McClelland (2000). However, it is important to realize that K_1 decreases continuously to zero at T_k, but that at T_v the behaviour of the magnetocrystalline anisotropy is discontinuous. Therefore low-temperature demagnetization is expected to occur either continuously on approach to T_k, or discontinuously at T_v.

Another implication not previously considered is the orientation of the *c*-axis. On cooling through the Verwey transition, the magnetite structure changes from inverse spinel to monoclinic. The monoclinic unit cell consists of four rhombohedrally distorted cells. In these cells, the *c*-axis is aligned 0.24° from the cubic [001]-axis (Fig. 1), and so the *c*-axis may align in one of four possible directions on cooling through the Verwey transition (Otsuka & Sato 1986). The small misalignment from the [001]-axis also slightly distorts the lattice cell, giving rise to a spontaneous strain in the monoclinic phase (Salje 1993). To reduce the net spontaneous strain of a grain, it can be energetically favourable for different areas of a grain to have their *c*-axes aligned in different directions. Each area with the *c*-axis uniformly orientated is termed a twin domain, and the boundaries between twin domains are called twin-domain boundaries (Salje 1993). The relationship between spontaneous strain and twin domains is analogous in many respects to the formation of magnetic domain walls in an attempt to reduce the net spontaneous magnetization. As the spontaneous strain is zero above T_v, in terms of its elastic properties the Verwey transition is often referred to as a ferroelastic transition (e.g. Medrano *et al.* 1999). Thus, on cooling through the Verwey transition, twin domains may be created.

In zero magnetic field, twin-domain structures have widths of about 100–200 μm, so it should be expected that only larger multidomain grains will display such twin-domain structures. However, in the presence of high magnetic fields (~ 400 mT), the twin-domain walls can re-order themselves to reduce the net magnetization (Medrano *et al.* 1999). On reordering in high magnetic fields, twin-domain structures can have twin-domain widths as low as ~ 20 μm. Hence, the magnetic domains and twin-domain walls interact, in agreement with theory (Houchmandzadeh *et al.* 1991). This may have implications for hysteresis curves measured in multidomain magnetite below the Verwey transition, which may be affected by this interaction.

Variations in stress and stoichiometry affect the temperature of the Verwey transition. The temperature of T_v decreases with both stress and non-stoichiometry. It is postulated that stress fields around dislocations will give rise to a range of Verwey-transition temperatures in a sample. The temperature of T_k is affected by non-stoichiometry; however, the rate of decrease is less than that for T_v.

ACKNOWLEDGMENTS

This work was carried out during the tenure of a NERC research studentship to ARM. We thank Eduard Petrovsky and an anonymous reviewer for helpful reviews. The measurements were carried out at the Institute for Rock Magnetism, University of Minnesota, and the Departments of Chemistry at the Universities of Edinburgh and Oxford. We are grateful to the relevant universities for the use of their facilities.

REFERENCES

Abe, K., Miyamoto, Y. & Chikazumi, S., 1976. Magnetocrystalline anisotropy of low-temperature phase of magnetite, *J. Phys. Soc. Japan,* **41,** 1894–1902.

Abrikosov, A.A., 1968. Formulation of bound states of conduction-electron with localised spins in metals, *Sov. Phys. JETP,* **26,** 641–646.

Aksenova, E.V., Gorbach, V.N. & Mamalui, V.N., 1987. Investigation of magnetostriction of magnetite near the Verwey temperature, *Sov. Phys. Solid State,* **29,** 1149–1152.

Alperin, H.A., Steinsvoll, O., Nathans, R. & Shirane, G., 1967. Magnon scattering of polarised neutrons by the diffraction method: measurements on magnetite, *Phys. Rev.,* **154,** 508–514.

Anderson, P.W., 1956. Ordering and antiferromagnetism in ferrites, *Phys. Rev.,* **102,** 1008–1013.

Aragón, R., 1992. Magnetisation and exchange in non-stoichiometric magnetite, *Phys. Rev. B,* **46,** 5328–5333.

Aragón, R., Buttrey, D.J., Shepherd, J.P. & Honig, J.M., 1985. Influence of non-stoichiometry on the Verwey transition, *Phys. Rev. B,* **31,** 430–436.

Arai, K.I., Ohmori, K., Tsuya, N. & Iida, S., 1976. Magnetostriction of magnetite in the vicinity of the low-temperature transition, *Phys. Stat. Sol. (a),* **34,** 325–330.

Belov, K.P., 1993. Electronic processes in magnetite (or 'Enigmas in magnetite'), *Physics-Uspekhi,* **36,** 380–391.

Belov, K.P., 1994. Anomalies of the magnetoresistance of ferrites, *Physics-Uspekhi,* **37** (6), 563–575.

Belov, K.P., 1996a. Ferrimagnets with a 'weak' magnetic sublattice, *Physics-Uspekhi,* **39,** 623–634.

Belov, K.P., 1996b. On the nature of a low-temperature transition in magnetite, *JETP,* **36,** 1152–1155.

Belov, K.P., Goryaga, A.N., Pronin, V.N. & Skipetrova, L.A., 1982. Spin-reorientation transition in magnetite as an example of spinodal decomposition in a magnetic system, *JETP Lett.,* **36,** 146–149.

Belov, K.P., Goryaga, A.N., Sheremet'ev, V.N. & Naumova, O.A, 1985. The nature of the small contribution to the magnetostriction of Fe^{2+} ions in spinel, *JETP Lett.,* **42,** 117–119.

Bickford, L.R., 1949. Ferromagnetic resonance absorption in magnetite, *Phys. Rev.,* **76,** 137–138.

Bickford, L.R., 1950. Ferromagnetic resonance absorption in magnetite single crystals, *Phys. Rev.,* **78,** 449–457.

Bickford, L.R., Brownlow, J.M. & Penoyer, R.F., 1957. Magnetocrystalline anisotropy in cobalt-substituted magnetic single crystals, *Proc. I.E.E.,* **B104,** 238–244.

Calhoun, B.A., 1954. Magnetic and electric properties of magnetite at low-temperatures, *Phys. Rev.,* **94,** 1577–1585.

Chainani, A., Yokoya, T., Morimoto, T., Takahashi, T. & Todo, S., 1996. Electronic structure of Fe_3O_4 across the Verwey transition, *J. Electron Spect. Rel. Phen.,* **78,** 99–102.

Cullen, J.R. & Callen, E.E., 1971. Band theory of multiple ordering and the m*et al.*-semiconductor transition in magnetite, *Phys. Rev. Lett.,* **26,** 236–238.

Cullen, J.R. & Callen, E., 1973. Multiple ordering in magnetite, *Phys. Rev. B,* **7,** 397–402.

Dankers, P. & Sugiura, N., 1981. The effects of annealing and concentration on the hysteresis properties of magnetite around the PSD–MD transition, *Earth planet. Sci. Lett.,* **56,** 422–428.

De Grave, E., Persoons, R.M., Vanderberghe, R.E. & de Bakker, P.M.A., 1993. Mössbauer study of the high-temperature phase of Co-substituted magnetites, $Co_xFe_{3-x}O_4$, I. $x \geq 0.04$, *Phys. Rev. B,* **47,** 5881–5893.

Domenicali, C.A., 1950. Magnetic and electric properties of natural and synthetic single crystals of magnetite, *Phys. Rev. B,* **78,** 459–467.

Dunlop, D.J. & Özdemir, Ö., 1997. *Rock Magnetism: Fundamentals and Frontiers,* Cambridge University Press.

Fletcher, E.J. & O'Reilly, W., 1974. Contribution of Fe^{2+} ions to the magnetocrystalline anisotropy constant K_1 of $Fe_{3-x}Ti_xO_4$ $(0 < x < 0.1)$, *J. Phys. C,* **7,** 171–178.

Gleitzer, C., 1997. Electrical properties of anhydrous iron oxides, *Key Eng. Mat.,* **125–126,** 355–418.

Gridin, V.V., Hearne, G.R. & Honig, J.M., 1996. Magnetoresistance extremum at the first-order Verwey transition in magnetite (Fe_3O_4), *Phys. Rev. B,* **53,** 15 518–15 521.

Hargrove, R.S. & Kündig, W., 1970. Mössbauer measurements of magnetite below the Verwey transition, *Solid State Comm.,* **8,** 303–308.

Heider, F. & Bryndzia, L.T., 1987. Hydrothermal growth of magnetite crystals (1 μM to 1 mm), *J. Crystal Growth,* **84,** 50–56.

Heider, F., Zitzelsberger, A. & Fabian, K., 1996. Magnetic-susceptibility and remanent coercive force in grown magnetite crystals from 0.1 μm to 6 mm, *Phys. Earth planet. Inter.,* **93,** 239–256.

Hodych, J.P., 1990. Magnetic hysteresis as a function of low temperature in rocks: evidence for internal stress control of remanence in multi-domain and pseudo-single-domain magnetite, *Phys. Earth planet. Inter.,* **64,** 21–26.

Honig, J.M., 1995. Analysis of the Verwey transition in magnetite, *J. Alloys Compounds,* **229,** 24–39.

Honig, J.M. & Spalek, J., 1992. Elementary formulation of the Verwey transition in magnetite via order-disorder formalism, *J. Solid State Chem.,* **96,** 115–122.

Houchmandzadeh, B., Lajzerowicz, J. & Salje, E., 1991. Order parameter coupling and chirality of domain walls, *J. Phys. condens. Matter,* **3,** 5163–5169.

Iida, S., 1980. Structure of at Fe_3O_4 low temperature, *Phil. Mag. B,* **42,** 349–376.

Isida, S., Suzuki, M., Todo, S., Môri, T. & Siratori, K., 1996. Pressure effect on the elastic constants of magnetite, *Physica B,* **219** and **220,** 638–640.

Kakol, Z., 1990. Magnetic and transport properties of magnetite in the vicinity of the Verwey transition, *J. Solid State Chem.,* **88,** 104–114.

Kakol, Z. & Honig, J.M., 1989. Influence of deviations from ideal stoichiometry on the anisotropy parameters of magnetite $Fe_{3-\delta}O_4$, *Phys. Rev. B,* **40,** 9090–9097.

Kakol, Z., Sabol, J. & Honig, J.M., 1991. Magnetic anisotropy of titanomagnetites $Fe_{3-x}Ti_xO_4$, $0 \leq X \leq 0.55$, *Phys. Rev. B,* **44,** 2198–2204.

King, J., 1996. Magnetic properties of arrays of magnetite particles produced by the method of electron beam lithography (EBL), *PhD thesis,* University of Edinburgh.

Kittel, C., 1949. Physical theory of ferromagnetic domains, *Rev. mod. Phys,* **21,** 541–583.

Kobayashi, K. & Fuller, M., 1968. Stable remanence and memory of multidomain materials with special reference to magnetite, *Phil. Mag.,* **18,** 601–624.

Kozlowski, A., Kakol, Z., Kim, D., Zalecki, R. & Honig, J.M., 1996. Heat capacity of $Fe_{3-\alpha}M_\alpha O_4$ (M = Zn, Ti, $0 \leq \alpha \leq 0.$ 04), *Phys. Rev. B,* **54,** 12 093–12 098.

Lee, E.W., 1955. Magnetostriction and magnetomechanical effects, *Rept. Prog. Phys.,* **18,** 184–229.

Matsui, M., Todo, S. & Chikazumi, S., 1977. Magnetisation of the low temperature phase of Fe_3O_4, *J. Phys. Soc. Japan,* **43,** 47–53.

McClelland, E. & Shcherbakov, V.P., 1995. Metastability of domain state in MD magnetite: consequences for remanence acquisition, *J. geophys. Res.,* **100(B3),** 3841–3857.

Medrano, C., Schlenker, M., Baruchel, J., Espeso, J. & Miyamoto, Y., 1999. Domains in the low-temperature phase of magnetite from synchroton-radiation X-ray topographs, *Phys. Rev. B,* **59,** 1185–1195.

Millar, R.W., 1929. The heat capacities at low-temperature of Ferrous Oxide magnetite and cuprous and cupric oxides, *J. Am. chem. Soc.,* **51,** 215–222.

Mishra, S.K. & Satpathy, S., 1993. Energetic stabilisation of the Mizoguchi structure for magnetite by band-structure effects, *Phys. Rev. B,* **47,** 5564–5570.

Miyamoto, Y. & Chikazumi, S., 1988. Crystal symmetry of magnetite in low temperature phase deduced from magnetoelectric measurement, *J. Phys. Soc. Japan,* **57,** 2040–2050.

Mizoguchi, M., 1978a. NMR Study of the low-temperature phase of Fe_3O_4. I. Experiments, *J. Phys. Soc. Japan,* **44,** 1501–1511.

Mizoguchi, M., 1978b. NMR Study of the low-temperature phase of Fe_3O_4. II. Electron ordering analysis, *J. Phys. Soc. Japan,* **44,** 1512–1520.

Moloni, K., Moskowtiz, B.M. & Dahlberg, E.D., 1996. Domain structures in single crystal magnetite below the Verwey transition as observed with a low-temperature magnetic force microscope, *Geophys. Res. Lett.,* **23,** 2851–2854.

Moskowitz, B.M., Frankel, R.B. & Bazylinski, D.A., 1993. Rock magnetic criteria for the detection of biogenic magnetite, *Earth planet. Sci. Lett.,* **120,** 283–300.

Moskowitz, B.M., Jackson, M. & Kissel, C., 1998. Low-temperature magnetic behaviour of titanomagnetites, *Earth planet. Sci. Lett.,* **157,** 141–149.

Mulay, L.N. & Boudreaux, U., 1976. *Theory and Application of Molecular Diamagnetism,* Wiley-Interscience, New York.

Muxworthy, A.R. & McClelland, E., 2000. The causes of low-temperature demagnetization of remanence in multidomain magnetite, *Geophys. J. Int.,* **140,** 115–131 (this issue).

Muxworthy, A.R. & Williams, W.W., 2000. Micromagnetic models of pseudo-single domain grains of magnetite near the Verwey transition, *J. geophys. Res.,* in press.

Nagaev, É.L., 1971. Conductivity of magnetic semiconductors in the case of strong coupling between carriers and localised spins, *Sov. Phys. Solid State,* **13,** 961–967.
Okudera, H., Kihara, K. & Matsumoto, T., 1996. Temperature dependence of structure parameters in natural magnetite: Single crystal X-ray study from 126 K and 773 K, *Acta. Cryst.,* **B52,** 450–457.
O'Reilly, W., 1984. *Rock and Mineral Magnetism,* Blackie and Sons Ltd, Glasgow.
Otsuka, N. & Sato, H., 1986. Observation of the Verwey transition in Fe_3O_4 by high-resolution electron microscopy, *J. Solid State Chem.,* **61,** 212–222.
Özdemir, Ö. & Dunlop, D.J., 1998. Single-domain-like behaviour in a 3-mm natural single crystal of magnetite, *J. geophys. Res.,* **103**(B2), 2549–2562.
Rave, W., Fabian, K. & Hubert, A., 1998. The magnetic states of small cubic magnetic particles with uniaxial anisotropy, *J. Magn. magn. Mater.,* **190,** 332–348.
Rozenberg, G.Kh., Hearne, G.R., Pasternak, P.M., Metcalf, P.A. & Honig, J.M., 1996. Nature of the Verwey transition in magnetite (Fe_3O_4) to pressures of 16 GPa, *Phys. Rev. B,* **53,** 6482–6487.
Rubinstein, M. & Forester, P.W., 1971. Investigation of the insulating phase magnetite by NMR and the Mössbauer effect, *Solid State Comm.,* **9,** 1675–1679.
Sahu, S., 1997. An experimental study on the effects of stress on the magnetic properties of magnetite, *PhD thesis,* University of Minnesota.
Sahu, S. & Moskowitz, B.M., 1995. Thermal dependence of magnetocrystalline anisotropy and magnetostriction constants of single crystal $Fe_{2.4}Ti_{0.61}O_4$, *Geophys. Res. Lett.,* **22,** 449–452.
Salje, E.K.H., 1993. *Phase Transitions in Ferroelastic and Co-Elastic Crystals,* Cambridge University Press, Cambridge.
Samiullah, M., 1995. Verwey transition in magnetite: Finite-temperature mean-field solution of the Cullen–Callen model, *Phys. Rev. B,* **51,** 10 352–10 356.
Schmidbauer, E. & Keller, R., 1996. Magnetic properties and rotational hysteresis of Fe_3O_4 and γ-Fe_2O_3 particles 500 nm in diameter, *J. Magn. magn. Mater.,* **152,** 99–108.
Siratori, K. & Kino, Y., 1980. A note on the magnetic anisotropy of Fe_3O_4, *J. Magn. magn. Mater.,* **20,** 87–90.
Skipetrova, L.A., 1978. Effect of cation-cation exchange on the magnetic properties of ferrites with spinel structure, *PhD thesis,* Moscow State University (in Russian).
Slonczewski, J.C., 1958. Origin of magnetic anisotropy in $Co_xFe_{3-x}O_4$, *J. appl. Phys.,* **29,** 448–449.
Syono, Y., 1965. Magnetocrystalline anisotropy and magnetostriction of Fe_3O_4-Fe_2TiO_4 series—with special application to rock magnetism, *Japan. J. Geophys.,* **4,** 71–143.
Thompson, R. & Oldfield, F., 1986. *Environmental Magnetism,* Allen and Unwin Publishers, London.
Torrie, B.H., 1967. Spin-waves in magnetite at a temperature below the electronic ordering transition, *Solid State Comm.,* **5,** 715–717.
Toyoda, T., Sasaki, S. & Tanaka, M., 1999. Evidence for charge ordering of Fe^{2+} and Fe^{3+} in magnetite observed by synchrotron X-ray anomalous scattering, *Am. Min.,* **84,** 294–298.
Träuble, H., 1969. The influence of crystal defects on magnetisation processes in ferromagnetic single crystals, in *Magnetism and Metallurgy,* pp. 621–687, eds Berkowitz, A.E. & Kneller, E., Academic Press, San Diego.
Tsuya, N., Arai, K.I. & Ohmori, K., 1977. Effect of magnetoelastic coupling on the anisotropy of magnetite below the transition temperature, *Physica,* **86–88B,** 959–961.
Verwey, E.J.W., 1939. Electronic conduction of magnetite (Fe_3O_4) and its transition point at low-temperature, *Nature,* **44,** 327–328.
Verwey, E.J.W. & Haayman, P.W., 1941. Electronic conductivity and transition point of magnetite ('Fe_3O_4'), *Physica,* **VIII (9),** 979–987.
Verwey, E.J.W. & Heilmann, E.L., 1947. Physical properties and cation arrangement of oxides with spinel structures. I. Cation arrangement in spinels, *J. Chem. Phys.,* **15,** 174–180.
Verwey, E.J.W., Haayman, P.W. & Romeijn, F.C., 1947. Physical properties and cation arrangement of oxides with spinel structures. II. Electronic conductivity, *J. Chem. Phys.,* **15,** 181–187.
Vonsovskii, S.V., 1946. On the exchange interaction of the valence and inner electrons in ferromagnetic (transition) metals, *J. Phys.,* **10,** 468–475.
Walz, F. & Kronmüller, H., 1991. Evidence for a single-stage Verwey transition in perfect magnetite, *Phil. Mag. B,* **64,** 623–628.
Walz, F. & Kronmüller, H., 1994. Analysis of magnetic point-defect relaxations in electron-irradiated magnetite, *Phys. Stat. Sol. (B),* **181,** 485–498.
Yama-ai, M., Ozima, M. & Nagata, T., 1963. Self-reversal of remanent magnetisation of magnetite at low-temperature, *Nature,* **197,** 444–445.
Ye, J., Newell, A.J. & Merrill, R.T., 1994. A re-evaluation of the magnetocrystalline anisotropy and magnetostriction constants, *Geophys. Res. Lett.,* **21,** 25–28.
Yoshida, J. & Iida, S., 1979. X-ray study of the phase transition in magnetite, *J. Phys. Soc. Japan,* **47,** 1627–1633.
Zhang, Z. & Satpathy, S., 1991. Electron states, magnetism and the Verwey transition, *Phys. Rev. B,* **44,** 13 319–13 331.
Zuo, J.M., Spence, J.C.H. & Petuskey, W., 1990. Charge ordering in magnetite, *Phys. Rev. B,* **42,** 8451–8464.

APPENDIX A: DESCRIPTION OF SAMPLES

Although this paper is effectively a review paper, three samples were used in the remanence experiments: these were MD synthetic samples made by A. R. Muxworthy using the hydrothermal recrystallization technique described by Heider & Bryndzia (1987). Grain size distributions and magnetic parameters of the samples are summarized in Table A1. The samples had slightly wider grain distributions than the hydrothermal crystals prepared by Heider & Bryndzia (1987). XRD analysis and Mössbauer spectroscopy confirmed that these samples were pure magnetite. The hyperfine splitting was observed using a batch of Johnson–Matthey magnetite that was non-stoichoimetric and contained small amounts of maghemite and haematite.

Table A1. Summary of mean grain size, standard deviation σ, hysteresis parameters coercive force (H_c), remanent coercive force (H_{cr}) and the ratio of the saturation remanence (M_{rs}) to the saturation magnetization (M_{sat}) at room temperature, for the samples considered in this study. *H* (3.0 μm)–*H* (76 μm) are multidomain hydrothermal samples.

sample name	size (μm)	$\pm\sigma$ (μm)	H_c (mT)	H_{cr}	M_{rs}/M_{sat}
H (3.0 μm)	3.0	2.4	2.4	26.5	0.018
H (39 μm)	39	9	1.5	24.7	0.010
H (76 μm)	76	25	0.96	19.9	0.006